biomass

MDPI

Article

Effect of Process Parameters and Biomass Type on Properties of Carbon Produced by Pyrolysis

Sourabh Chakraborty [1], Nazlim Aktay [1], Fikret Muge Alptekin [2], Melih Soner Celiktas [2] and Nurhan Turgut Dunford [1,3,*]

[1] Department of Biosystems and Agricultural Engineering, Oklahoma State University, Stillwater, OK 74078, USA
[2] Solar Energy Institute, Ege University, Izmir 35100, Turkey
[3] Robert M. Kerr Food & Agricultural Products Center, Stillwater, OK 74078, USA
* Correspondence: nurhan.dunford@okstate.edu; Tel.: +1-405-744-7062

Abstract

Porous carbon from renewable resources like biomass is a key material utilized in many applications ranging from environmental remediation to energy storage. There are limited reports in the literature on the effects of biomass pretreatment, production process parameters, and downstream processing on the final product properties. This is the first study aimed at closing the latter research gap. Six different types of underutilized biomass were examined: eastern red cedar wood, pecan shells, hazelnut shells, algal biomass, miscanthus, and sludge produced at municipal wastewater treatment facilities. Although pretreatment of biomass with KOH or $ZnCl_2$ enhanced formation of micro- and mesopores, carbon yield was lower (15.3–32.5%) than that obtained via non-catalytic pyrolysis (28.3–48%). An optimization study performed using response surface methodology and cedar wood has shown the significant effects ($p < 0.05$) of temperature and catalyst/biomass ratio on total BET pore volume and surface area. Additionally, catalyst/biomass ratio had a significant effect on the crystal structure and pore size distribution in the carbon produced by pyrolysis. Hence, optimization of process temperature, hold time, and activation ratio is capable of yielding porous carbon from cedar wood pyrolysis with desirable properties.

Keywords: high porosity carbon; cedar wood; RSM; SEM; XRD; type II adsorption isotherms

check for updates

Academic Editors: Shaohua Jiang, Changlei Xia, Shifeng Zhang and Xiaoshuai Han

Received: 2 June 2025
Revised: 24 July 2025
Accepted: 7 August 2025
Published: 1 September 2025

Citation: Chakraborty, S.; Aktay, N.; Alptekin, F.M.; Celiktas, M.S.; Dunford, N.T. Effect of Process Parameters and Biomass Type on Properties of Carbon Produced by Pyrolysis. *Biomass* **2025**, *5*, 52. https://doi.org/10.3390/biomass5030052

Copyright: © 2025 by the authors. Licensee MDPI, Basel, Switzerland. This article is an open access article distributed under the terms and conditions of the Creative Commons Attribution (CC BY) license (https://creativecommons.org/licenses/by/4.0/).

1. Introduction

Porous carbon materials exhibit excellent performance in many energy- and environment-related applications because of their distinctive properties such as large specific surface area and pore volume, unique morphology, controllable pore structure, and good thermal, chemical, and mechanical strength. Porous carbon with desirable properties for specific applications can be synthesized by one of the following techniques: hard-, soft-, in situ, multi-, or self-templating, salt melt, or activation. Yet, cost of porous carbon synthesis tends to be high [1,2].

Porous carbon can also be produced from biomass. In recent decades, emphasis on biobased material production and utilization has been increasing due to the tremendous pressure on non-renewable resources and their adverse impact on the environment and human health. Biomass is a renewable resource that may alleviate the demand on non-renewable supplies [3]. Total biomass across all living organisms on Earth is estimated to be about 550 Gt C (gigatons of carbon, 1 Gt C = 1015 g of carbon) of which about 80%

(about 450 Gt C) are plants [4–6]. Hence, biomass is a clean, abundant, and renewable resource that plays a critical role not only in support of ecological systems but also in meeting our material needs. Responsible use of available biomass is the key for sustainable development. Circular bioeconomy and biorefinery concepts are based on sustainable conversion of biomass to various products by adding value to underutilized biomass and minimizing waste [7].

Biomass based carbon has been widely utilized for water and wastewater treatment and flue gas upgrading for decades. Relatively new interests in clean energy and biomass based industrial product manufacturing expanded potential availability and use of carbon produced from biomass in many other applications ranging from soil remediation, heat and power generation, metallurgical applications, greenhouse gas sequestration, and building material manufacturing to energy storage [8–10].

Biomass-derived porous carbon materials can be produced by pyrolysis, hydrothermal carbonization, soft- and hard-templating, and mechanochemical syntheses [11]. Pyrolysis of biomass produces gas and liquid streams along with a solid material commonly referred to as biochar. During the pyrolysis process, parts of the biomass decompose while a large portion of its carbon content is retained. Feedstock used, pyrolysis process conditions, biomass pretreatment, and downstream processing of the produced carbon significantly affect physical and chemical properties as well as yield of the final product. Although there are previous studies examining various aspects of biochar produced from different types of biomass [12–17], most of those reports lack an in-depth characterization of the starting material and evaluation of the effects of biomass type, presence or lack of pretreatment, conversion process parameters, downstream processing, and their interactions on the final product properties and yield.

Eastern red cedar is considered an invasive plant species in Oklahoma causing degradation of grasslands, water absorption from soil, and displacement of native wildlife and plant species [18]. It is expected that pyrolysis of this material will produce higher value products than the current methods used to control the problem, burning or utilizing it in very low value applications such as gardening aid.

Large amounts of sludge are generated during municipal wastewater treatment. Concerns about the adverse effects of conventional disposal methods and presence of metals with high thermal and electrical conductivity (Cr, Cu, Ni, Zn, Fe) in sludge makes it a good potential feedstock for non-edible applications such as carbon production via pyrolysis [19,20].

In recent decades, microalgal biomass has been receiving a lot of attention as a feedstock for bioproduct manufacturing. Algal biomass, specifically when grown in wastewater, could be a better feedstock than the biomass from terrestrial plants because of the faster growth rate and lower nutrient requirement of algae cultivation. Furthermore, algal biomass production does not require agricultural land eliminating the competition with availability of agricultural land for food, fiber, and feed production [21].

Shells separated from edible kernels of tree nuts are byproducts of the nut shelling industry and are usually marketed as a gardening aid (mulch), which is a low value application. About 40 to 50% of the whole nut weight is comprised of shells [22]. Pecan (*Carya illinoinensis*) trees are native to the United States and grown in all the southern states, including Oklahoma. Turkey is one of the largest producer and processor of hazelnuts. Hence, pecan and hazelnut shells are valuable resources for local value-added processing initiatives.

The main objective of this study is to optimize a pyrolysis process that will maximize pore volume, surface area, and yield of carbon produced from locally available, but un-

derutilized, biomass and evaluate effect of the production process parameters on the final product properties.

2. Materials and Methods

2.1. Materials

Biomass samples, tree nut shells (pecan and hazelnut shells), red cedar wood, and digested sludge generated at municipal wastewater treatment facilities were obtained directly from local processors. Algal biomass used in this study was grown in animal wastewater in our laboratories at Oklahoma State University, Stillwater, OK, USA (36.1224° N 97.0698° W), using a mixed consortium of the following 15 strains of microalgae purchased from the Culture Collection of Algae at the University of Texas (UTEX), Austin, TX, USA (30.285° N 97.735° W): *Navicula* sp. SP 11, *Tetraselmis striata* SP 22, *Aphanothece* sp. SP 25, *Geitlerinema amphibium* SP 27, *Geitlerinema carotinosum* SP 28, *Komvophoron* sp. SP 33, *Phormidium keutzingianum* SP 38, *Pseudanabena* sp. SP 46, *Pseudanabena* sp. SP 47, *Pseudanabena* sp. SP 48, *Dunaliella* sp. SP19, *Dunaliella* sp. SP 20, *Aphanocapsa* sp. SP 23, *Tychonema bornetii* SP 50, and *Picochlorum oklahomensis* [23,24]. All the chemicals used in the experiments were reagent grade unless otherwise stated.

2.2. Methods

The analyses of dry matter, ADF (Acid Detergent Fiber), NDF (Neutral Detergent Fiber), and mineral contents (standard ICP method) for all of the 6 biomasses were carried out using the forage analysis testing techniques as described by Fulgueria et al. [25]. The ADL (Acid Detergent Lignin) amount in the biomass samples was determined according to Kouisni and Paleologou [26].

Proximate analyses for all the biomass samples examined in this study were performed using a TGA instrument (Perkin Elmer; TGA 4000 Series, MA, USA) based on the method reported by Zhou and Dunford [27]. The experiments were carried out in duplicate and relative standard deviation in mean values for all the analytical data was less than 7% unless otherwise stated in the data tables.

2.3. Carbon Production

The pyrolysis experiments (average heating rate of about 10 °C/min) were carried out with and without biomass pretreatment. For the biomass pretreatment, one-liter solutions were prepared by dissolving the required amount of catalyst, either $ZnCl_2$ or KOH, needed for each activation ratio (0, 1:1, 2:1 and 4:1 catalyst: biomass weight ratio) in water.

$ZnCl_2$ is a commonly used chemical for biomass activation. This can be attributed to its ability to act as a Lewis acid, which helps in dehydrating the biomass, thereby favoring charring and aromatization reactions that lead to creation of a porous structure [28]. Besides $ZnCl_2$, KOH is another chemical activation agent that can be used for biomass activation. It is known to create porous carbons in the range of microporous (pore diameter < 2 nm) and ultra-microporous carbons (pore diameter < 1 nm) [29]. This is potentially known to enhance CO_2 adsorption. So, pyrolysis of biomass activated using KOH can be expected to be environment-friendly. Thus, activation agents of $ZnCl_2$ and KOH were chosen for this study.

The biomass samples (each 750 g of ground biomass) selected for activation were mixed with the aqueous catalyst solutions at the desired activation ratio and the slurry was stirred at room temperature (22 °C) for 24 h. Then, the slurry was transferred to a glass tray and dried at 110 °C in a vacuum oven until constant weight was reached. The catalyst-treated and dried biomass samples were stored in separate clean glass containers until further use in pyrolysis experiments.

The optimization study was carried out using eastern red cedar wood (pure and activated with $ZnCl_2$ catalyst) according to the experimental design (Box-Behnken Design; BBD) shown in Table 1 in a 6-inch (1.52×10^{-3} m) diameter horizontal ceramic cylindrical tube furnace (Mellen 3 NACCI, Mellen Company Inc., Concord, NH, USA). BBD is a form of response surface methodology (RSM) modeling, which offers advantages over other forms of experimental design like central composite design and full factorial design. These include fewer experimental points within the operational range of experimental parameters examined, fewer number of tests for establishing the experimental design, less labor-intensive, etc. Hence, RSM modeling in the form of BBD was chosen for experimental design [30,31].

Table 1. Experimental design, yield, surface area, and pore volume of the carbon produced from red cedar wood by pyrolysis (pure feedstock and that activated with $ZnCl_2$).

Run Order	Input Pyrolysis Parameters			Pyrolysis Process Output		
	Temperature (°C)	Hold Time (h)	Activation Ratio *	Carbon Yield (%)	Surface Area (m^2/g)	Pore Volume × 10^6 (m^3/g)
1	900	2	2	15.3	1578.6	1.0
2	900	2	0	28.3	215.1	0.15
3	900	1	1	21.5	1014.5	0.61
4	500	3	1	32.1	252.7	0.18
5	500	2	0	48.0	15.1	0.02
6	500	1	1	30.3	6.0	<0.01 (0.004)
7	700	1	0	32.0	17.5	0.02
8	700	2	1	26.2	1267.5	0.71
9	700	1	2	17.1	1774.6	1.14
10	900	3	1	24.7	969.9	0.6
11	500	2	2	19.2	326.95	0.22
12	700	3	0	32.5	27.2	0.03
13	700	2	1	24.9	1204	0.75
14	700	3	2	15.5	1952.1	1.24
15	700	2	1	24.4	1414.7	0.86

* Activation Ratio refers to Catalyst: Biomass (eastern red cedar wood) ratio on a weight: weight basis.

The feedstock sample was placed in a ceramic crucible placed in the center of the furnace. The quantity of feedstock sample placed in the crucible varied based on the activation ratio. So, for a pure cedar wood sample, about 375 g of sample was used. For activation ratios of 1 and 2, approximately 750 and 1125 g of sample were used, respectively, such that about 375 g of pure cedar wood biomass was present in these activated samples. Before beginning the pyrolysis experiments, the feedstock sample placed in the crucible was purged with N_2 for about 5 min to ensure an inert environment.

Downstream processing of the carbon samples was carried out by mixing the samples in 1 M HCl (at an acid/carbon weight ratio of 6) for 4 h followed by washing the acid-treated samples with deionized water, until the wash water pH was over 6.5. Then the neutralized samples were dried at 100 °C until a constant weight was reached. Washed and dried samples were stored in separate clean glass containers until further use.

2.4. Characterization of Porous Carbon

The BET (Brunauer–Emmett–Teller) surface area of the produced carbon was analyzed using N_2 adsorption/desorption isotherms at −196 °C (Autosorb iQ-C-XR, Anton Paar, Ashland, VA, USA). Overnight degassing (12–16 h) was employed between experiments.

The microstructure of carbon obtained from pyrolysis of eastern red cedar wood at 700 °C, 3 h, and a catalyst/biomass ratio of 2 was analyzed by Scanning Electron Microscopy

(SEM) using a FEI Quanta 600 field emission gun environmental SEM (Fischer Scientific, Waltham, MA, USA).

FTIR analysis of the cedar-wood-based carbon was performed without any sample pretreatment using a Lyza7000 (Anton Paar, Ashland, VA, USA) spectrophotometer in attenuated total reflectance (ATR) mode with a germanium crystal. Solid samples were placed directly on the ATR crystal, and spectra were recorded over the wavenumber range of 4000 to 525 cm^{-1}, with a fresh background collected for each run. The resolution was set to 4 cm^{-1}, and each spectrum was obtained from 48 scans.

Crystal structure of the carbon sample was evaluated by XRD scanning 2θ (two-theta) in degrees from 15° to 85° for 60 s (AXS D8 Discover XRD, Bruker, Billerica, MA, USA).

2.5. Statistical Analyses

Data analyses were performed using Minitab v 22.1 (2025; Academic License, online version), Minitab LLC, State College, PA, USA.

3. Results and Discussion

3.1. Biomass Chemical Properties

The chemical composition of biomass used for porous carbon production has significant effects on the properties and performance of the final product. Hence, biomass samples examined in this study, pecan nut and hazelnut shells, sludge, miscanthus, eastern red cedar wood, and algal biomass, were characterized by analyzing their proximate and elemental compositions as well as their mineral contents. As expected, dry matter contents of the samples were very high ranging from 79.7 to 93.7% (Table 2). Because of the higher moisture content in algal biomass (16.5%) than in the other samples (4.5–9%), the lowest dry matter content was found in algal biomass (79.7%). Fiber content of the samples, specifically relative amounts of cellulose, hemicellulose, and lignin, has a significant effect on the amount and properties of the carbon produced through pyrolysis. Higher lignin content in biomass tends to promote carbonization and results in a higher carbon content in biochar. Table 2 shows ADF, NDF, and ADL of the samples. ADF represents cell wall components of the material, mainly cellulose and lignin contents. Algal biomass and sludge had very low ADF, while the other samples examined in this study contained higher ADF values ranging from 63% to 69.9%. Miscanthus had the highest NDF, 83.4%, which is a measure of the total cell wall content, including hemicellulose, cellulose, and lignin. Pecan and hazelnut shells had higher ADL values than the other samples because of the higher lignin content in the nut shells. Fiber content of the microalgal biomass used in this study was lower than that reported in the literature for strains *Chlamydomonas reinhardtii* [32], *Ulva lactuca* and *Cladophora glomerata* [33], and *Chlorella pyrenoidosa* and *Spirulina platensis* [34]. The latter result is due to the differences in properties of algal strains and growth conditions. The NDF contents of all the lignocellulosic feedstock used in this study except miscanthus (65.9–74.7 wt%) were less than that of Guinea Grass (81 wt%). Miscanthus (83.4 wt%) had a similar NDF content as Guinea Grass [35]. The NDF contents of pecan (65.9 wt%) and hazelnut shell (67.5 wt%) used in this study were lower than that of corn straw (70–72 wt%) and microalgae—containing corn straw reported in other publications [36].

Higher volatile content in biomass leads to the formation of greater amounts of liquid and gas products, lowering the residual carbon yield from pyrolysis. Among the samples evaluated in this study, algal biomass had the lowest amount of volatile matter: 45.6%. Fixed carbon content of a biomass represents the solid, combustible residue left after volatile matter is driven off [37,38]. Nut shells had higher fixed carbon content than the other samples evaluated. Total carbon value is the sum of both the organic and inorganic carbon forms in a sample. The algal biomass and sludge had lower total carbon content

that other samples, partly due to the higher nitrogen (protein) content in these samples. Nitrogen, sulphur, carbon, hydrogen, and oxygen contents of the biomass determine their suitability for a given conversion technique, i.e., biomass with high nitrogen and sulphur content is not the best material for pyrolysis because nitrogen and sulphur in biomass are converted into environmentally harmful gases during biomass degradation [34,39].

Table 2. Chemical composition (wt %) of the biomass samples [a].

Biomass/Parameter	Cedar Wood	Miscanthus	Pecan Shell	Hazelnut Shell	Microalgae	Sludge
Dry matter	92.1	93.6	86.6	89.3	79.7	93.7
ADF	69.9	63	68.6	69.6	9.6	ND [a]
NDF	74.7	83.4	65.9	67.5	10.4	ND
ADL	28.9	14.1	42.1	33.9	1.9	ND
Moisture	6.8	5.1	9	8.2	16.5	4.5
Volatile Matter	68.5	75.1	62.5	62.8	45.6	52.4
Ash	3.7	2.8	2.4	4.6	27.3	29.4
C	47.8	46.5	47.7	46	25.3	47.8
H	5.5	5.9	5.5	5.4	4.6	5.5
N	0.6	0.4	0.9	1.3	5.4	0.6
S	0.2	3	9	2.9	5.4	0.2
O	42.2	41.4	34.6	39.8	32.1	42.2

[a] ND: Not detected, ADF: Acid Detergent Fiber, ADL: Acid Detergent Lignin, NDF: Neutral Detergent Fiber.

Mineral composition of the biomass also affects its pyrolysis profile and final product properties, specifically the solid product properties. Metal contents (Fe, Zn, Mg) of municipal wastewater sludge were significantly higher than that of the other samples (Table 3). Heavy metals, Ni, Cr, and Pb, were detected only in the sludge sample. The amount of Cd and As in the samples was below the detection limit of the analytical method used for the tests.

Table 3. Mineral content (ppm) of the biomass from various sources.

Element/ Biomass	Cedar Wood	Miscanthus	Pecan Shell	Hazelnut Shell	Microalgae	Sludge
P	220	610	640	50,080	380	19,590
Ca	6560	1190	5760	1900	6050	35,680
K	680	3050	5350	44,450	2040	3290
Mg	360	430	940	36,540	590	5160
Na	440	10	20	33,570	20	5370
S	480	310	720	5160	310	17,510
Fe	1622	26	675	555	24	13,119
Zn	29	19	21	21	10	1124
Cu	4	-	7	5	4	618

Table 3. *Cont.*

Element/ Biomass	Cedar Wood	Miscanthus	Pecan Shell	Hazelnut Shell	Microalgae	Sludge
Mn	158	176	119	21	78	471
B	-	-	7	3	-	19
Ni	-	-	-	-	3	21
Cr	-	-	-	-	-	28
Pb	-	-	-	-	-	49

3.2. Process Optimization

Studies carried out in our laboratory with six different biomass types (Table 4) have demonstrated the significant effects of biomass type, biomass pretreatment method, pyrolysis process parameters, and downstream processing of the biochar on the final product properties.

Table 4. Effect of carbon production process parameters on surface area and total pore volume.

Biomass Type	Temperature (°C)	Catalyst	Catalyst Ratio	Downstream Process	Surface Area (m^2/g)	Pore Volume × 10^6 (m^3/g)
Hazelnut Shell	No pyrolysis	$ZnCl_2$	1:1	Acid/water wash	1.69	0.02
Hazelnut Shell	450	$ZnCl_2$	1:1	Acid/water wash	1170.05	0.61
Hazelnut Shell	450	$ZnCl_2$	1:1	Water wash	946.14	0.52
Hazelnut Shell	600	$ZnCl_2$	1:1	Acid/water wash	1226.9	0.63
Hazelnut Shell	450	$ZnCl_2$	1:4	Acid/water wash	1050.8	0.6
Hazelnut Shell	600	$ZnCl_2$	1:4	Acid/water wash	1186.88	0.87
Hazelnut Shell	450	KOH	1:1	Acid/water wash	343.6	0.21
Hazelnut Shell	600	KOH	1:1	Acid/water wash	489.77	0.29
Hazelnut Shell	450	-	-	Acid/water wash	103.19	0.07
Hazelnut Shell	600	-	-	Acid/water wash	436.44	0.24
Hazelnut Shell	600	$ZnCl_2$	1:2	Acid/water wash	1904.41	0.52
Cedar Wood	600	$ZnCl_2$	1:2	Acid/water wash	1944.65	0.51
Pecan Nut Shell	600	$ZnCl_2$	1:2	Acid/water wash	1346.19	0.35
Microalgae	600	$ZnCl_2$	1:2	Acid/water wash	1017.74	0.01
Sludge	600	$ZnCl_2$	1:2	Acid/water wash	645.57	0.3
Microalgae/Sludge /Cedar Wood Mix	600	$ZnCl_2$	1:2	Acid/water wash	1236.83	0.62
Miscanthus	600	$ZnCl_2$	1:4	Acid/water wash	1449	1.32

Pretreatment of biomass with a catalyst is critical for enhancing pore formation in the solid material produced during pyrolysis. The experiments carried out with hazelnut shells (Table 4) clearly show that non-catalytic pyrolysis produces solid materials with a total pore volume and surface area that are several orders of magnitude lower than those obtained with KOH or $ZnCl_2$ pretreatment of biomass. Furthermore, the type and amount of activator/catalyst added to biomass determine the surface composition and structure of the carbon produced. Pore volume and surface area of the solid pyrolysis product increase as the catalyst/biomass ratio increases. The experimental data shown in Table 4

suggest that $ZnCl_2$ is a more effective activator/catalyst than KOH for increasing total BET pore volume in carbon produced from the biomass examined in this study. Downstream processing of the carbon produced via pyrolysis by treating the product with acid followed by washing with deionized water until neutrality enhances total pore volume by removing acid-soluble components and flushing out the deposits remaining in the pores. Lower cellulose and lignin and higher protein contents of sludge and algal biomass resulted in low total pore volume [40–42]. Hence, they are not suitable for porous carbon production.

A pyrolysis process optimization study carried out with miscanthus was published earlier [43]. In the latter study, a lower temperature (450–750 °C) and time (30–90 min) and a higher catalyst/biomass ratio (0–4:1) range were examined. Considering that a larger catalyst/biomass ratio adds to the operating cost and reduces production capacity by taking up reactor space that otherwise could be used for biomass loading, the current study limited the biomass/catalyst ratio to 1:2 and examined a higher temperature range and residence time. Based on the data collected with six different biomass types (Table 4), eastern red cedar was selected for process optimization. Eastern red cedar wood is an inexpensive, locally available, and underutilized resource. Furthermore, the high carbon, fiber, and lower nitrogen and sulphur contents of eastern red cedar wood (Table 1) make it a good candidate for producing porous carbon through pyrolysis. Because of its high pore volume creation activity, $ZnCl_2$ was chosen for biomass pretreatment in the current study. The chemical mechanism of biomass activation with $ZnCl_2$ to enhance porosity has been reported in other publications [44,45].

The Box–Benken experimental design shown in Table 4 was used for data collection. Red cedar wood pyrolysis process parameters, temperature, activation ratio, and time, were optimized for maximum carbon yield, total pore volume, and surface area, and a combination of carbon yield/pore volume/surface area by Surface Response Method (SRM).

The surface plots (Figure 1a–c) show that increasing temperature and activation ratio improved total pore volume (BET volume) of the produced carbon. Time did not have a significant effect on the pore volume (p = 0.22). Statistical analysis of the experimental data (Table 5) also confirmed that only the effects of temperature, activation ratio, and temperature × temperature interaction (quadratic effect of temperature) had significant effects on pore volume at p = 0.05 level. Similar to the results obtained for total volume, temperature and activation ratio were positively correlated with surface area; as the temperature and activation ratio increased, surface area increased (Figure 1d–f). The effect of hold time on area was not significant (p = 0.69). For the carbon yield, temperature, activation ratio, and temperature × activation ratio interaction were significant. The following Surface Response models were generated for total BET pore volume and surface area.

$$Total\ Pore\ Volume = -4.72 + 0.0128 \times Temperature + 0.4237 \times Activation\ Ratio - 8 \times 10^{-6} \times Temperature \times Temperature \quad (1)$$

$$Surface\ Area = 7759 + 21.12 \times Temperature + 670 \times Activation\ Ratio - 0.0137 \times Temperature \times Temperature \quad (2)$$

The models for surface area (F = 14.17, p = 0.0, and R^2 = 85.01%) and pore volume (F = 15.29, p = 0.0, and R^2 = 85.95%) were significant and lack of fit was insignificant.

The model for the yield was not significant (F = 1.12, p = 0.48), indicating that determination of the optimum conditions for maximizing yield requires refinement in the Box–Benken design used. It is possible that the temperature range chosen for the evaluation was too broad. Higher pyrolysis temperatures used in this study lowers the carbon yield and produces more volatile products. The optimum conditions that resulted in the highest pore volume, surface area, yield, and their combinations are shown in Table 6.

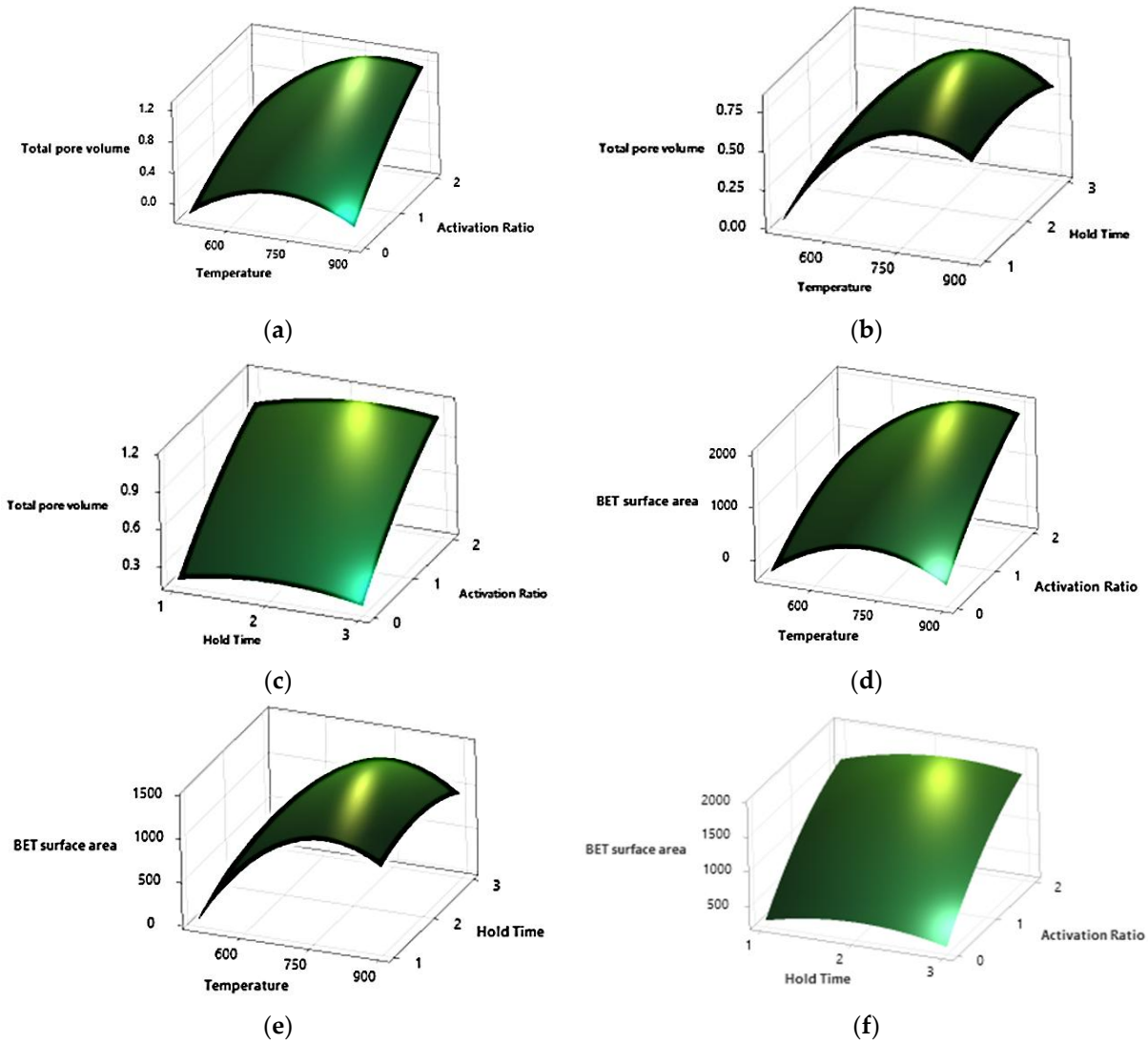


Figure 1. Surface plots for total pore volume and surface area for biochar obtained from eastern red cedar wood pyrolysis. [Pore Volume and Surface Area affected by: (**a**,**e**) Temperature and Activation Ratio; (**b**,**d**) Temperature and Hold Time; (**c**,**f**) Hold Time and Activation Ratio, respectively].

Table 5. ANOVA table for total volume, surface area, and carbon yield.

Parameter		Surface Area		Total Pore Volume		Carbon Yield	
Source	**DF**	**F-Value**	***p*-Value**	**F-Value**	***p*-Value**	**F-Value**	***p*-Value**
Model	**4**	14.17	0.0	15.29	0.0	20.44	<0.01
Linear	**3**	15.38	0.0	16.8	0.0	55.45	0.0
Temperature	**1**	11.96	<0.01	12.37	<0.01	37.48	<0.01
Hold Time	**1**	0.18	0.68	0.26	0.62	0.36	0.58
Activation Ratio	**1**	33.99	0.0	37.77	0.0	128.52	0.0
Temperature × Temperature	**1**	10.57	<0.01	10.76	<0.01	4.44	0.09
Hold Time × Hold Time	**1**	0.91	0.38	0.55	0.49	0.57	0.48
Activation Ratio × Activation Ratio	**1**	1.24	0.32	0.59	0.48	0.09	0.78

Table 5. *Cont.*

Parameter		Surface Area		Total Pore Volume		Carbon Yield	
Source	**DF**	**F-Value**	***p*-Value**	**F-Value**	***p*-Value**	**F-Value**	***p*-Value**
Temperature × Hold Time	**1**	0.20	0.68	0.19	0.68	0.09	0.77
Temperature × Activation Ratio	**1**	2.58	0.17	2.40	0.18	11.81	0.02
Hold Time × Activation Ratio	**1**	0.07	0.81	0.05	0.82	0.21	0.67
Lack-of-Fit	**8**	11.4	0.09	6.84	0.13	5.94	0.15

Table 6. Optimum process parameters for maximizing carbon yield, surface area, and total pore volume.

Process Parameter/Response	Temperature (°C)	Hold Time (h)	Activation Ratio
Surface Area	774.75	3	2
Total Volume	772.95	3	2
Yield	500.0	3	1.66
Surface Area/Total Volume	673.74	3	2
Surface Area/Total Volume/Yield	774.75	3	2

3.3. Characteristics of the Carbon Produced from Cedar Wood

BET surface area, total pore volume, pore size distribution, product yield, and carbon and mineral contents of the carbon samples were examined to evaluate the potential applications for the products. The highest final product yield, 48%, was obtained at 500 °C, 2 h of pyrolysis time, and an activation ratio of 0 (carbon obtained after downstream treatment of the pyrolysis biochar with acid followed by neutralization with deionized water washing) (Table 4). A lower pyrolysis temperature and time in the absence of a catalyst contributes to lower biomass conversion rates, resulting in higher amounts of residual solid material. The highest total BET pore volume, 1.24×10^{-6} m^3/g, and surface area, 1952.1 m^2/g, were attained at 700 °C, 3 h of heat treatment, and with the highest activation ratio, 2, examined in this study. The previous experiments conducted with miscanthus indicate a similar trend: lack of biomass pretreatment with $ZnCl_2$ results in higher yields but lower surface area and total pore volume [43].

In this article, IUPAC pore size definitions are used as follows: (a) macropores: pores with pore widths exceeding about 50 nm, (b) mesopores: pores of widths between 2 nm and 50 nm, and (c) micropores: pores with widths not exceeding about 2 nm [46]. Pore size distribution in high porosity carbon is one of the most important criteria determining its performance in various applications, especially for controlling the performance of the composite materials made by infusing PCM in porous carbon [47]. For example, it has been reported that mesopores have a lower electrosorption density in capacitive deionization applications and ion selectivity can be controlled by engineering the ratio of mesoporosity to microporosity in carbon [48]. Interests in porous carbon produced from sustainable resources for shape stabilization of phase change materials (PCM) designed for energy storage applications have been increasing [49,50].

Figure 2a–c show the effect of the production process parameters on the nitrogen adsorption/desorption hysteresis of the carbon produced from eastern red cedar wood.

Figure 2d,e represents the IUPAC classification of adsorption/desorption isotherms and hysteresis loops [51].

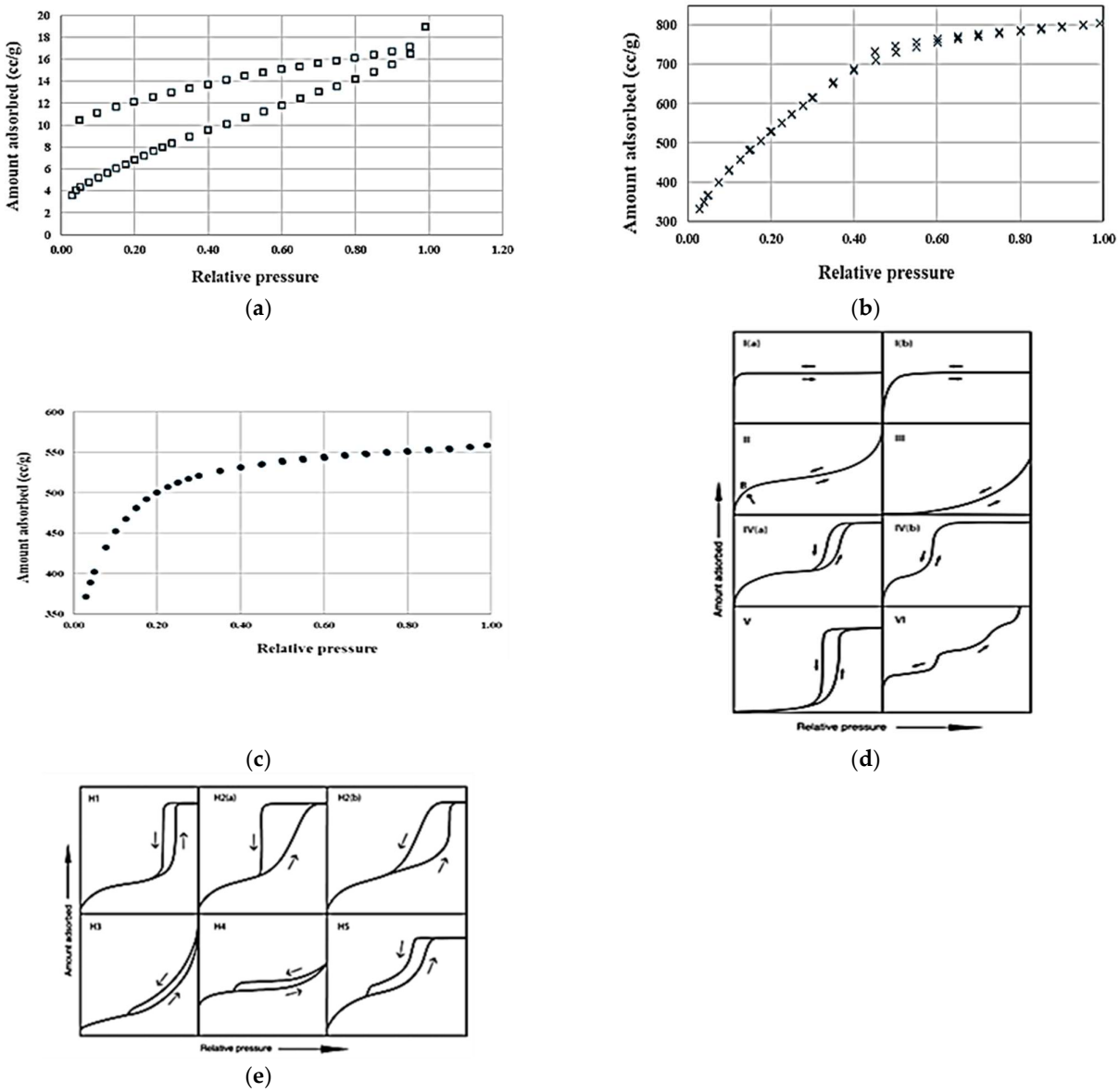


Figure 2. Effect of processing conditions on the nitrogen adsorption/desorption profile of the carbon sample produced from eastern red cedar wood at 700 °C with or without $ZnCl_2$ treatment. (**a**): No $ZnCl_2$ pretreatment, (**b**): $ZnCl_2$ treatment at 1:1 $ZnCl_2$/biomass ratio and (**c**): $ZnCl_2$ treatment at 2:1 $ZnCl_2$/biomass ratio (**d**,**e**): Adsorption Isotherms.

The nitrogen gas adsorption and desorption isotherms of the carbon produced from cedar wood without $ZnCl_2$ pretreatment (Figure 2a) resembles the IUPAC classification Type II isotherm indicating a macroporous structure [51]. An irreversible type of hysteresis loop indicates strong bonding of gas molecules to functional groups on the carbon surface, resisting desorption. This shape is due to the unrestricted monolayer–multilayer adsorption up to a high relative partial pressure. The gradual curvature is an indication of a significant amount of overlap of monolayer coverage and the onset of multilayer adsorption, and the thickness of the adsorbed multilayer generally appears to increase without limit until the partial pressure reaches 1. Barrett, Joyner, and Halenda (BJH) pore size distribution analysis indicated that the pores ranging 3.4–122.8 nm in width had a total pore volume of 0.01×10^{-6} m^3/g and surface area of 5.55 m^2/g. Total volume and surface area of the same

sample (1.5–24 nm pore width) analyzed by the Non-Local-Density Functional Theory (NLDFT) were 0.02 × 10^{-6} m^3/g and 26.08 m^2/g, respectively. Micropores (pore width less than 2 nm) comprised of about 45.7% of the pore volume (Figure 3a).

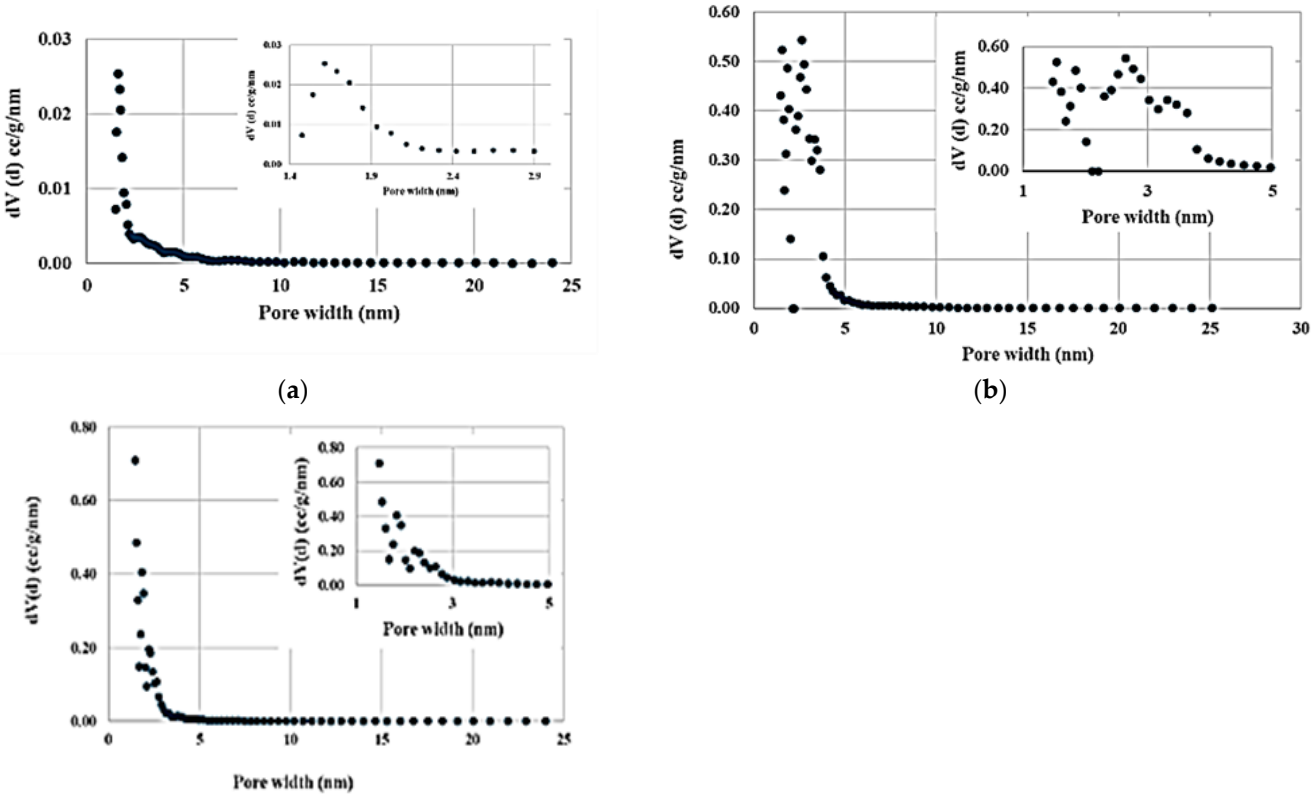


Figure 3. Pore size distribution of carbon produced from eastern red cedar wood pyrolysis at 700 °C and different catalyst/biomass ratios: (**a**) no catalyst, (**b**) catalyst/biomass ratio of 1:1, and (**c**) catalyst/biomass ratio of 2:1.

The carbon produced with $ZnCl_2$ pretreatment (Figure 2b,c) displayed reversible physisorption Type Ib isotherm. These materials tend to have a pore size distribution over a broad range including wide micropores and may be narrow mesopores. The amount of gas adsorbed approached a limiting value that is governed by the accessible micropore volume rather than by the internal surface area. A steep gas uptake at very low partial pressures, specifically for the sample produced at 700 °C, 3 h, and an activation ratio of 2, in Figure 2c is due to enhanced adsorbent–adsorptive interactions in narrow micropores [51]. The latter sample had a significantly higher total BET pore volume (1.24 × 10^{-6} m^3/g) and surface area than the other samples. Catalyst addition widens the pore width, hence, micropore volume comprised only 38.8% of the total volume of this sample (Figure 3c).

Elemental and mineral contents of the pyrolysis product show that (Table 7) about 59% of the material consisted of carbon. Relatively high Zn content in the porous carbon is due to the residual from $ZnCl_2$ pretreatment of biomass prior to pyrolysis. The SEM imaging of the carbon produced at 700 °C, 3 h, and an activation ratio of 2 (Figure 4) confirms the broad and irregular pore width distribution in the sample.

Table 7. Composition of carbon produced from cedar wood at 700 °C, 3 h, and catalyst/biomass ratio of 2.

Element	P	Ca	K	Mg	Na	S	Fe	Zn	Cu	Mn	B	Ni	Al	N	C
Unit	(ppm)													(%)	
Amount	10	40	0	0	0	450	78	128	7	1	0	7	302	0.52	58.90

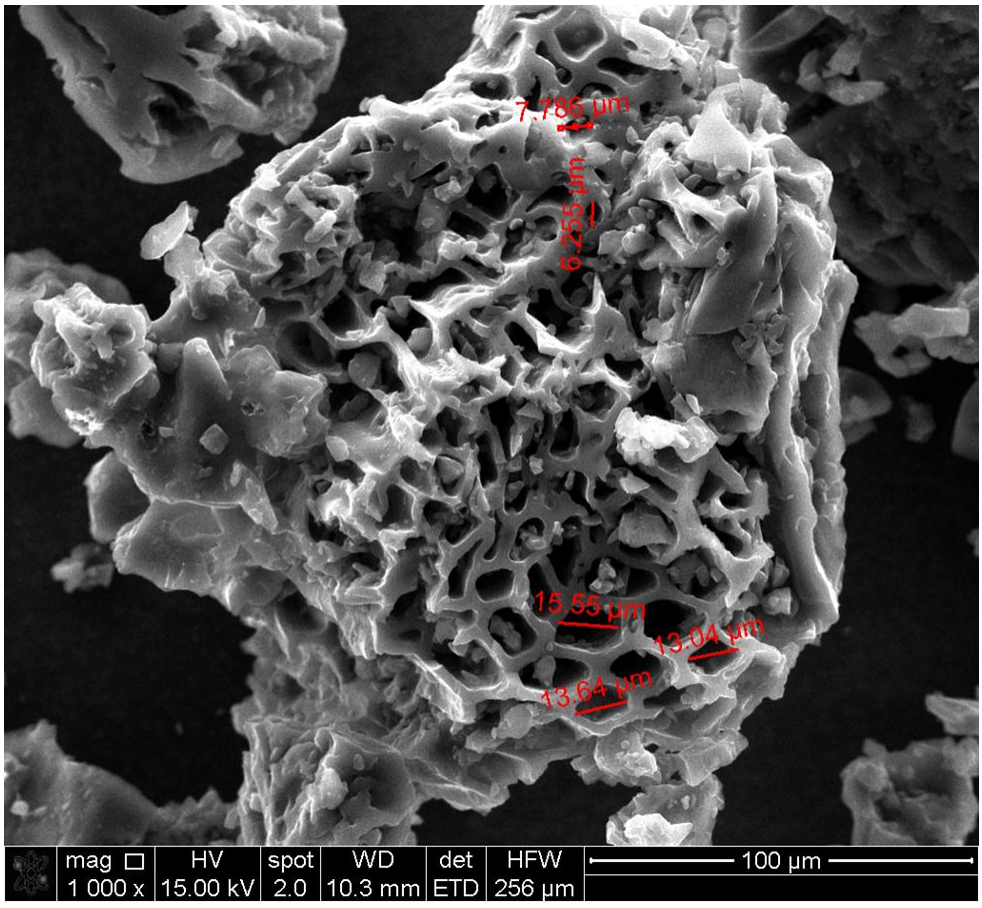


Figure 4. SEM imaging of the carbon sample produced from eastern red cedar wood pyrolysis at 700 °C, 3 h, and activation ratio of 2.

FTIR spectrum of the carbon produced at 700 °C, 3 h, and an activation ratio of 2 (Figure 5) did not show large peaks, only broad small transmittance between wavelength 1750 and 1000 cm^{-1} that correspond, C=C, C-N, and C-H stretching. High temperature pyrolysis promotes decomposition of the material, breaking up the functional groups on the material [52]. The very small peak at about 2966 cm^{-1} is attributed to aliphatic CH_n stretching vibration. The observed peak at 1670 cm^{-1} represents carbonyl and carboxyl groups. The bands at 1250 cm^{-1} are assigned to C–O stretching.

The XRD plots for the carbon produced at 700 °C with different catalyst/biomass ratios (Figure 6) clearly show the effect of catalyst on the crystal structure of the final product. The peaks at 20.7 and 26.5 were common to all three products but peak intensities varied. The peak at 20.7 is usually attributed to carbon, kaolinite, and hydrated compounds. Crystalline forms of silica (quartz, cristobalite) and graphite appear around 26.5 2Theta. Metal oxides or specific crystallographic planes of minerals usually appear around 39.5° and 68.2°. The catalyst/biomass ratio increased intensity of the first peak corresponding to amorphous carbon at 20.7 as well as the second peak attributed to graphite form, appearing

at 26.5 2Theta, which indicates that catalytic pyrolysis not only impacts the micro- and meso-sized pore distribution but also crystal structure of the product.

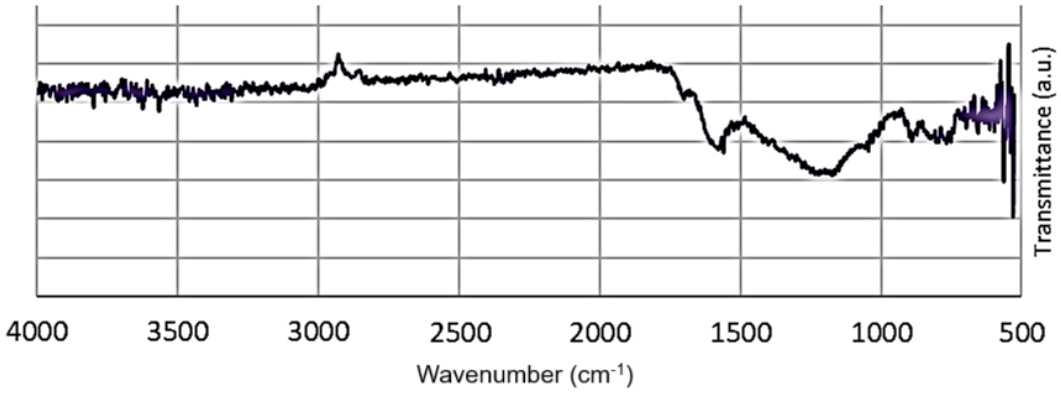
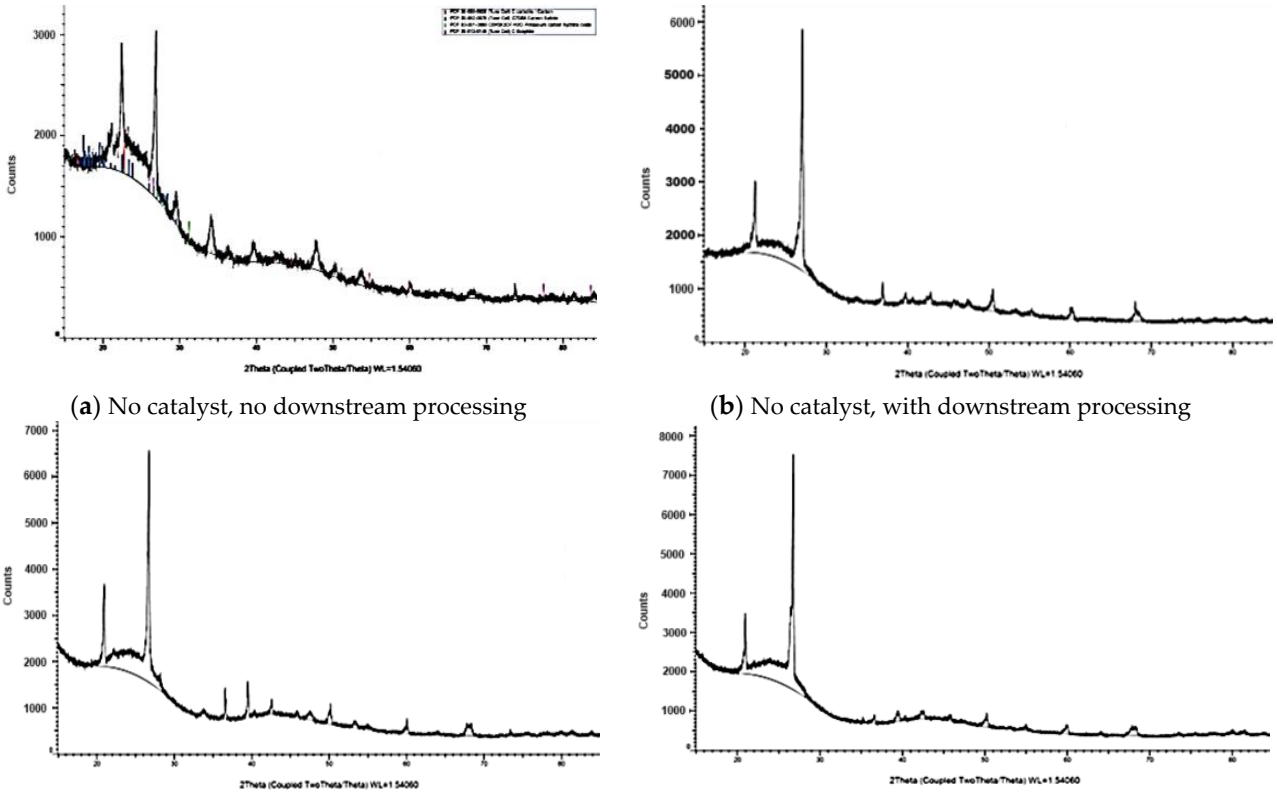


Figure 5. FTIR spectrum of the carbon produced from red cedar wood at 700 °C, 3 h, and catalyst/biomass ratio of 2.



(**a**) No catalyst, no downstream processing

(**b**) No catalyst, with downstream processing

(**c**) Catalyst/biomass ratio of 1:1 with downstream processing

(**d**) Catalyst/biomass ratio of 1:2 with downstream processing

Figure 6. Effect of catalyst ratio and downstream processing on the XRD of the carbon produced from red cedar wood at 700 °C.

4. Conclusions

This is the first extensive study examining the effects of the type of biomass and production process parameters on physical and chemical properties of the carbon produced via pyrolysis. The experimental data presented in this study establish that temperature and catalyst/biomass weight ratio have significant effects on carbon yield, total pore volume, and surface area while the effect of pyrolysis time is insignificant. Pretreatment of biomass

with a catalyst prior to pyrolysis was crucial for producing high porosity carbon. The experiments carried out with KOH and $ZnCl_2$ as catalysts indicate that $ZnCl_2$ was more effective in promoting pore formation than KOH. Pyrolysis process parameters can be customized to produce high porosity carbon with desirable characteristics suitable for specific applications. Although, converting underutilized low value materials such as eastern red cedar wood and nut shells, to high porosity carbon by catalytic pyrolysis is a simple and relatively inexpensive method, and downstream processing of the produced carbon with acid treatment followed by water washing improves pore volume; the entire process utilizes a large amount of catalyst, consumes huge volumes of fresh water, and generates wastewater. Hence, a lifecycle analysis of the process is necessary to determine potential environmental impact and sustainability of the process examined in this study.

This study focused on the maximization of total pore volume and surface area of carbon produced from an underutilized resource, eastern red cedar, via pyrolysis. The high porosity carbon having a 1952.1 cm^2/g BET surface area and 1.24×10^{-6} m^3/g total pore volume was successfully produced (pyrolysis at 700 °C; hold time = 3 h; activation ratio = 2) and characterized by evaluating its physical and chemical properties. Ongoing research is investigating the potential application of the latter product in thermal energy storage applications, i.e., shape stabilization of organic phase change materials used in thermal energy storage. Yet, pyrolysis carbon has many other applications in electronics and construction material manufacturing.

Author Contributions: Conceptualization: N.T.D.; Methodology: S.C., F.M.A., N.T.D. and M.S.C.; Validation: N.T.D. and M.S.C.; Formal Analysis: N.T.D. and M.S.C.; Investigation: S.C., F.M.A., N.A., N.T.D. and M.S.C.; Methodology: S.C., F.M.A., N.T.D. and M.S.C.; Validation: N.T.D. and M.S.C.; Resources, N.T.D. and M.S.C.; Data Curation: S.C., F.M.A. and N.A.; Writing—Original Draft Preparation: N.T.D.; Writing—Review & Editing: S.C., F.M.A., N.T.D. and M.S.C.; Supervision: N.T.D. and M.S.C.; Project Administration, N.T.D.; Funding Acquisition, N.T.D. and M.S.C. All authors have read and agreed to the published version of the manuscript.

Funding: This project is funded by the US Department of Agriculture, National Institute of Food and Agriculture (NIFA) South Central Sun Grant Program. During this work, Fikret Muge Alptekin was supported by the Scientific and Technological Research Council of Turkey (TUBITAK) with a scholarship under 2211-C National PhD Scholarship Program in the Priority Fields in Science and Technology and 2214-A International Doctoral Research Fellowship Program. This work was also supported by Ege University Scientific Research.

Institutional Review Board Statement: Not applicable.

Informed Consent Statement: Not applicable.

Data Availability Statement: The original contributions presented in this study are included in the article. Further inquiries can be directed to the corresponding author.

Acknowledgments: The authors of this manuscript are extremely thankful to the mentioned funding sources for providing the necessary fund in order to carry out this work.

Conflicts of Interest: The authors declare no conflicts of interest. The sponsors had no role in the design, execution, interpretation, or writing of the study.

References

1. Tian, W.; Zhang, H.; Duan, X.; Sun, H.; Shao, G.; Wang, S. Porous Carbons: Structure-Oriented Design and Versatile Applications. *Adv. Funct. Mater.* **2020**, *30*, 1909265. [CrossRef]
2. Yang, C.; Wang, K.; Lyu, W.; Liu, H.; Li, J.; Wang, Y.; Jiang, R.; Yuan, J.; Liao, Y. Nanofibrous Porous Organic Polymers and Their Derivatives: From Synthesis to Applications. *Adv. Sci.* **2024**, *11*, 2400626. [CrossRef] [PubMed]

3. Saeed, M.; Shahzad, U.; Fazle Rabbee, M.; Manzar, R.; Al-Humaidi, J.Y.; Siddique, A.; Sheikh, T.A.; Althomali, R.H.; Qamar, T.; Rahman, M.M. Potential Development of Porous Carbon Composites Generated from the Biomass for Energy Storage Applications. *Chem.—Asian J.* **2024**, *19*, e202400394. [CrossRef] [PubMed]
4. Bar-On, Y.M.; Phillips, R.; Milo, R. The Biomass Distribution on Earth. *Proc. Natl. Acad. Sci. USA* **2018**, *115*, 6506–6511. [CrossRef]
5. Doney, S.C.; Wolfe, W.H.; McKee, D.C.; Fuhrman, J.G. The Science, Engineering, and Validation of Marine Carbon Dioxide Removal and Storage. *Annu. Rev. Mar. Sci.* **2025**, *17*, 55–81. [CrossRef]
6. Wu, H.; Cui, H.; Fu, C.; Li, R.; Qi, F.; Liu, Z.; Yang, G.; Xiao, K.; Qiao, M. Unveiling the Crucial Role of Soil Microorganisms in Carbon Cycling: A Review. *Sci. Total Environ.* **2024**, *909*, 168627. [CrossRef]
7. Mesa, J.A.; Sierra-Fontalvo, L.; Ortegon, K.; Gonzalez-Quiroga, A. Advancing Circular Bioeconomy: A Critical Review and Assessment of Indicators. *Sustain. Prod. Consum.* **2024**, *46*, 324–342. [CrossRef]
8. Liu, W.-J.; Jiang, H.; Yu, H.-Q. Emerging Applications of Biochar-Based Materials for Energy Storage and Conversion. *Energy Environ. Sci.* **2019**, *12*, 1751–1779. [CrossRef]
9. Guo, M.; Song, W.; Tian, J. Biochar-Facilitated Soil Remediation: Mechanisms and Efficacy Variations. *Front. Environ. Sci.* **2020**, *8*, 521512. [CrossRef]
10. Yu, S.; He, J.; Zhang, Z.; Sun, Z.; Xie, M.; Xu, Y.; Bie, X.; Li, Q.; Zhang, Y.; Sevilla, M.; et al. Towards Negative Emissions: Hydrothermal Carbonization of Biomass for Sustainable Carbon Materials. *Adv. Mater.* **2024**, *36*, 2307412. [CrossRef]
11. Chakraborty, R.; Vilya, K.; Pradhan, M.; Nayak, A.K. Recent Advancement of Biomass-Derived Porous Carbon Based Materials for Energy and Environmental Remediation Applications. *J. Mater. Chem. A* **2022**, *10*, 6965–7005. [CrossRef]
12. Xing, T.; Yun, S.; Li, B.; Wang, K.; Chen, J.; Jia, B.; Ke, T.; An, J. Coconut-Shell-Derived Bio-Based Carbon Enhanced Microbial Electrolysis Cells for Upgrading Anaerobic Co-Digestion of Cow Manure and Aloe Peel Waste. *Bioresour. Technol.* **2021**, *338*, 125520. [CrossRef]
13. Hoffmann, V.; Rodriguez Correa, C.; Sachs, S.; del Pilar Sandoval-Rojas, A.; Qiao, M.; Brown, A.B.; Zimmermann, M.; Rodriguez Estupiñan, J.P.; Cortes, M.T.; Moreno-Piraján, J.C. Activated Carbon from Corncobs Doped with RuO2 as Biobased Electrode Material. *Electron. Mater.* **2021**, *2*, 324–343. [CrossRef]
14. kanthi Gudimella, K.; Gedda, G.; Kumar, P.S.; Babu, B.; Yamajala, B.; Rao, B.V.; Singh, P.P.; Kumar, D.; Sharma, A. Novel Synthesis of Fluorescent Carbon Dots from Bio-Based Carica Papaya Leaves: Optical and Structural Properties with Antioxidant and Anti-Inflammatory Activities. *Environ. Res.* **2022**, *204*, 111854. [CrossRef]
15. Lu, Q.; Zhou, S.; Li, B.; Wei, H.; Zhang, D.; Hu, J.; Zhang, L.; Zhang, J.; Liu, Q. Mesopore-Rich Carbon Flakes Derived from Lotus Leaves and It's Ultrahigh Performance for Supercapacitors. *Electrochim. Acta* **2020**, *333*, 135481. [CrossRef]
16. Redondo, E.; Carretero-González, J.; Goikolea, E.; Ségalini, J.; Mysyk, R. Effect of Pore Texture on Performance of Activated Carbon Supercapacitor Electrodes Derived from Olive Pits. *Electrochim. Acta* **2015**, *160*, 178–184. [CrossRef]
17. Zhang, X.; Zhang, K.; Li, H.; Cao, Q.; Li, P. Porous Graphitic Carbon Microtubes Derived from Willow Catkins as a Substrate of MnO_2 for Supercapacitors. *J. Power Sources* **2017**, *344*, 176–184. [CrossRef]
18. Dunford, N.; Hiziroglu, S.; Holcomb, R. Effect of Age on the Distribution of Oil in Eastern Redcedar Tree Segments. *Bioresour. Technol.* **2007**, *98*, 2636–2640. [CrossRef]
19. Fonts, I.; Gea, G.; Azuara, M.; Ábrego, J.; Arauzo, J. Sewage Sludge Pyrolysis for Liquid Production: A Review. *Renew. Sustain. Energy Rev.* **2012**, *16*, 2781–2805. [CrossRef]
20. Jacinto, G.S.S.; Cruz, G.; Cabral, A.A.; Bezerra, G.V.P.; Peña Garcia, R.R.; Magalhães, U.N.; Gomes, W.C. Biotechnological Investigation of Pediastrum Boryanum and Desmodesmus Subspicatus Microalgae Species for a Potential Application in Bioenergy. *Algal Res.* **2023**, *75*, 103266. [CrossRef]
21. Chakraborty, S.; Dunford, N.T. Algae: Nature's Renewable Resource for Fuels and Chemicals. *Biomass* **2024**, *4*, 329–348. [CrossRef]
22. Gur, C.S.; Dunford, N.T.; Gumus, Z.P. Cytotoxicity of Subcritical Water Extracts Obtained from Byproducts Generated at Commercial Pecan Shelling Operations on Cancer Cells. *Bioresour. Bioprocess* **2023**, *10*, 47. [CrossRef]
23. Chakraborty, S.; Dunford, N.T.; Goad, C. A Kinetic Study of Microalgae, Municipal Sludge and Cedar Wood Co-Pyrolysis. *Renew. Energy* **2021**, *165*, 514–524. [CrossRef]
24. Lutzu, G.A.; Concas, A.; Dunford, N.T. Characterization of Hypersaline Oklahoma Native Microalgae Cultivated in Flowback and Produced Water: Growth Profile and Contaminant Removal. *Bioprocess Biosyst. Eng.* **2024**, *47*, 665–681. [CrossRef] [PubMed]
25. Fulgueira, C.L.; Amigot, S.L.; Gaggiotti, M.; Romero, L.A.; Basílico, J.C. Forage Quality: Techniques for Testing. *Fresh Prod.* **2007**, *1*, 121–131.
26. Kouisni, L.; Paleologou, M. Method for Separating Lignin From Black Liquor. US8771464B2, 8 July 2014.
27. Zhou, N.; Dunford, N.T. Characterization of Green Microalgae and Cyanobacteria Isolated from the Great Salt Plains. *Trans. ASABE* **2017**, *60*, 283–290. [CrossRef]
28. Ullah, S.; Shah, S.S.A.; Altaf, M.; Hossain, I.; El Sayed, M.E.; Kallel, M.; El-Bahy, Z.M.; Rehman, A.U.; Najam, T.; Nazir, M.A. Activated Carbon Derived from Biomass for Wastewater Treatment: Synthesis, Application and Future Challenges. *J. Anal. Appl. Pyrolysis* **2024**, *179*, 106480. [CrossRef]

29. Patel, H.; Mohanty, A.; Misra, M. Post-Combustion CO_2 Capture Using Biomass Based Activated Porous Carbon: Latest Advances in Synthesis Protocol and Economics. *Renew. Sustain. Energy Rev.* **2024**, *199*, 114484. [CrossRef]
30. Roslan, S.Z.; Zainol, M.M.; Bikane, K.; Syed-Hassan, S.S.A. Hydrothermal Carbonization of Sewage Sludge for Hydrochar Production: Optimization of Operating Conditions Using Box-Behnken Design Coupled with Response Surface Methodology. *Biomass Convers. Biorefinery* **2025**, *15*, 10109–10125. [CrossRef]
31. Arroug, L.; Elaatmani, M.; Zegzouti, A. A Preliminary Study to Investigate the Beneficiation of Low-Grade Phosphate Sludge Using Reverse Flotation: Modeling and Optimization through Box-Behnken Design and Response Surface Methodology. *Chem. Eng. Res. Des.* **2024**, *204*, 228–237. [CrossRef]
32. Palangi, V.; Kaya, A.; Macit, M.; Nadaroglu, H.; Ünlü, H.B.; Kaya, A.; Fekri, A.; Mammadov, A.; Lackner, M. Comparative Anti-Methanogenic Ability of Green Algae (*C. reinhardtii*) with/without Nanoparticles: In Vitro Gas and Methane Production. *Front. Vet. Sci.* **2025**, *12*, 1492230. [CrossRef]
33. Sırakaya, S. Pros and Cons of Ulva Lactuca and Cladophora Glomerata Grown in Freshwater as Feed. *Environ. Sci. Pollut. Res.* **2023**, *30*, 33446–33454. [CrossRef]
34. Lobo, R.R.; Siregar, M.U.; da Silva, S.S.; Monteiro, A.R.; Salas-Solis, G.; Vicente, A.C.S.; Vinyard, J.R.; Johnson, M.L.; Ma, S.; Sarmikasoglou, E.; et al. Partial Replacement of Soybean Meal with Microalgae Biomass on in Vitro Ruminal Fermentation May Reduce Ruminal Protein Degradation. *J. Dairy Sci.* **2024**, *107*, 1460–1471. [CrossRef] [PubMed]
35. Alvarez-Guzmán, C.L.; Rodríguez-Hipólito, F.; Chávez-Reyes, Y.; Valdez-Vazquez, I. Lignocellulosic Biomass Mixtures Improve Hydrogen Production by Promoting Microbial Complementation in a Consolidated Bioprocess. *J. Clean. Prod.* **2025**, *489*, 144691. [CrossRef]
36. Wang, Z.; Wang, Z.; Wang, L.; Sun, D. Ammoniation of Filter Residues from Corn Straw Filtering the Microalgae Cultured in Urine Wastewater. *J. Environ. Manag.* **2025**, *377*, 124557. [CrossRef] [PubMed]
37. Diboma, B.S.; Atiotsia, V.H.; Che, L.C.; Essomba, P.B.; Bot, B.V.; Tamba, J.G. Gasification of Charcoal Derived from Tropical Wood Residues in an Updraft Fixed Bed Reactor. *Bioresour. Technol. Rep.* **2023**, *21*, 101308. [CrossRef]
38. Bowles, A.J.; Nievas, Á.; Fowler, G.D. Consecutive Recovery of Recovered Carbon Black and Limonene from Waste Tyres by Thermal Pyrolysis in a Rotary Kiln. *Sustain. Chem. Pharm.* **2023**, *32*, 100972. [CrossRef]
39. Adamczyk, J.; Smołka-Danielowska, D.; Krzątała, A.; Krzykawski, T. Chemical and Mineral Composition of Bottom Ash from Agri-Food Biomass Produced under Low Combustion Conditions. *Int. J. Environ. Sci. Technol.* **2024**, *21*, 4025–4036. [CrossRef]
40. Zhang, H.; Li, W.; Song, G.; Azad, S.A.; Madadi, M.; Deng, Z.; Samimi, A.; Sun, C.; Sun, F. Role of in Situ Surfactant Modification of Lignin Structure and Surface Properties during Glycerol Pretreatment in Modulating Cellulase-Lignin Binding Affinities. *J. Colloid Interface Sci.* **2025**, *687*, 786–800. [CrossRef]
41. Madhu, R.; Periasamy, A.P.; Schlee, P.; Hérou, S.; Titirici, M.-M. Lignin: A Sustainable Precursor for Nanostructured Carbon Materials for Supercapacitors. *Carbon* **2023**, *207*, 172–197. [CrossRef]
42. Liu, L.; Gao, Y.; Meng, H.; Pan, Q.; Wang, Z.; Zhou, Y.; Liu, B.; Cao, X. Pore-Scale, Mechanical, and Hydraulic Properties of EICP-Treated Sand Using Crude Legume Ureases with Different Protein Contents. *Acta Geotech.* **2024**, *19*, 4747–4763. [CrossRef]
43. Alptekin, F.M.; Dunford, N.T.; Celiktas, M.S. Miscanthus-Derived Energy Storage System Material Production. *ACS Omega* **2023**, *8*, 8779–8790. [CrossRef] [PubMed]
44. Zhou, Y.; Liu, J.; Shen, C.; Li, J.; Wang, T.; Xue, Y. Effect of Zinc Chloride-Modified Biochar with Varying Pore Structures on VOCs Inhibition and Pavement Performance of Asphalt. *Constr. Build. Mater.* **2025**, *472*, 140887. [CrossRef]
45. Guo, Z.; Han, X.; Zhang, C.; He, S.; Liu, K.; Hu, J.; Yang, W.; Jian, S.; Jiang, S.; Duan, G. Activation of Biomass-Derived Porous Carbon for Supercapacitors: A Review. *Chin. Chem. Lett.* **2024**, *35*, 109007. [CrossRef]
46. Kong, Z.; Zhang, H.; Zhou, T.; Xie, L.; Wang, B.; Jiang, X. Biomass-Derived Functional Materials: Preparation, Functionalization, and Applications in Adsorption and Catalytic Separation of Carbon Dioxide and Other Atmospheric Pollutants. *Sep. Purif. Technol.* **2025**, *354*, 129099. [CrossRef]
47. Zhang, K.; Hu, C.; Huang, H.; Li, B.; Huang, C.; Wang, S. Achieving Efficient Energy Utilization by PCM in the Food Supply Chain: Encapsulation Technologies, Current Applications, and Future Prospects. *J. Energy Storage* **2024**, *79*, 110214. [CrossRef]
48. Shih, Y.-J.; Wu, Z.-L.; Wang, M.-R.; Huang, C.-P. Catalytic Phase Transition of Cobalt Oxide Enriched in Mesoporous Carbon Polyhedrons for Electrosorption of Molybdate Oxyanions. *Chem. Eng. J.* **2025**, *518*, 164426. [CrossRef]
49. Mandal, S.; Ishak, S.; Mohd Ariffin, M.A.; Lee, D.-E.; Park, T. Effect of Pore Structure on the Thermal Stability of Shape-Stabilized Phase Change Materials. *J. Mater. Res. Technol.* **2023**, *25*, 465–479. [CrossRef]
50. Aktay, N. Evaluation of Low Value Lipids for Thermal Storage Applications. Master's Thesis, Oklahoma State University, Stillwater, OK, USA, 2025.

51. Thommes, M.; Kaneko, K.; Neimark, A.V.; Olivier, J.P.; Rodriguez-Reinoso, F.; Rouquerol, J.; Sing, K.S. Physisorption of Gases, with Special Reference to the Evaluation of Surface Area and Pore Size Distribution (IUPAC Technical Report). *Pure Appl. Chem.* **2015**, *87*, 1051–1069. [CrossRef]
52. Chen, Y.; Yang, H.; Wang, X.; Zhang, S.; Chen, H. Biomass-Based Pyrolytic Polygeneration System on Cotton Stalk Pyrolysis: Influence of Temperature. *Bioresour. Technol.* **2012**, *107*, 411–418. [CrossRef]

Disclaimer/Publisher's Note: The statements, opinions and data contained in all publications are solely those of the individual author(s) and contributor(s) and not of MDPI and/or the editor(s). MDPI and/or the editor(s) disclaim responsibility for any injury to people or property resulting from any ideas, methods, instructions or products referred to in the content.